



# 1 A new parameterization of the UV irradiance altitude 2 dependence for clear-sky conditions and its application in the 3 on-line UV tool over Northern Eurasia

4 N. Chubarova<sup>1</sup>, Ye. Zhdanova<sup>1</sup>, Ye. Nezval<sup>1</sup>

5 <sup>1</sup>Faculty of Geography, Moscow State University, GSP-1, 119991, Moscow, Russia

6 *Correspondence to:* Nataly Chubarova (chubarova@geogr.msu.ru)

7 **Abstract.** A new method for calculating the altitude UV dependence is proposed for different types of biologically  
8 active UV radiation (erythemally-weighted, vitamin-D-weighted and cataract-weighted types). We show that for the  
9 specified groups of parameters the altitude UV amplification ( $A_{UV}$ ) can be presented as a composite of independent  
10 contributions of UV amplification from different factors within a wide range of their changes with mean uncertainty  
11 of 1% and standard deviation of 3% compared with the exact model simulations with the same input parameters.  
12 The parameterization takes into account for the altitude dependence of molecular number density, ozone content,  
13 aerosol and spatial surface albedo. We also provide generalized altitude dependencies of the parameters for  
14 evaluating the  $A_{UV}$ . The resulting comparison of the altitude UV effects using the proposed method shows a good  
15 agreement with the accurate 8-stream DISORT model simulations with correlation coefficient  $r > 0.996$ . A  
16 satisfactory agreement was also obtained with the experimental UV data in mountain regions. Using this  
17 parameterization we analyzed the role of different geophysical parameters in UV variations with altitude. The  
18 decrease in molecular number density, especially at high altitudes, and the increase in surface albedo play the most  
19 significant role in the UV growth. Typical aerosol and ozone altitude UV effects do not exceed 10-20%. Using the  
20 proposed parameterization implemented in the on-line UV tool (<http://momsu.ru/uv/>) for Northern Eurasia over the  
21 PEEEX domain we analyzed the altitude UV increase and its possible effects on human health considering different  
22 skin types and various open body fraction for January and April conditions in the Alpine region.

23  
24 **Keywords:** UV radiation, altitude dependence, RT modelling, erythemally-weighted irradiance, vitamin D-weighted  
25 irradiance, cataract-weighted irradiance, interactive UV-tool.

## 26 1. Introduction

27 Biologically active UV radiation (BAUVR) is an important environmental factor, which significantly affect human  
28 health and nature (UNEP, 1998; UNEP, 2011). Enhanced levels of UV radiation lead to different types of skin  
29 cancer (basal and squamous cell carcinomas, cutaneous melanoma), to various eye diseases (cataract, photokeratitis,  
30 squamous cell carcinoma, ocular melanoma, variety of corneal/conjunctival effects), and to immunosuppression.  
31 However, small doses of UV radiation have a positive effect on health through the vitamin D generation (UNEP,  
32 2011).

33 UV radiation is affected by astronomical factors (solar zenith angle, solar-earth distance), by different atmospheric  
34 characteristics (total ozone content, cloudiness, aerosol, optically-effective gases), and by surface albedo (Bais et al.,  
35 2007, Bekki et al., 2011). However, the altitude above sea level has also a significant influence on UV radiation



36 (Bais et al., 2007). There are a lot of studies and special field campaigns in different geographical regions, which  
37 were devoted to the analysis of the altitude UV effect (Bernhard et al., 2008, Blumthaler and Ambach, 1988,  
38 Blumthaler et al., 1994, Blumthaler et al., 1997, Dahlback et al., 2007, Lenoble et al., 2004, Piacentini, et al. 2003,  
39 Pfeifer et al., 2006, Sola et al., 2008, etc.). The UV enhancement at high altitudes is detected not only due to smaller  
40 molecular scattering, but also due to usually observed decreasing in total ozone content and aerosol, and increasing  
41 in surface albedo, which in turn enhances 3D reflection from slopes of mountains covered by snow (Lenoble et al.,  
42 2004). In addition, variation of cloud properties with altitude can also change the level of UV radiation.

43 The UV records in mountainous areas demonstrate extremely high levels. The highest UV values are observed in  
44 Andes in Bolivia (Pfeifer et al., 2006, Zaratti et al., 2003), where the UV index can be sometimes close to 20. Very  
45 high UV levels were also recorded at high-altitude deserts in Argentina (Piacentini, et al. 2003). In Tibet the UV  
46 index frequently exceeded 15 on clear days and occasionally exceeded 20 on partially cloudy days (Dahlback et al.,  
47 2007). At the European alpine stations in summer conditions the UV indices are often higher than 11 (Hülse,  
48 2012). In winter, erythemally-weighted irradiance is about 60% higher than that at lower-altitude European sites  
49 (Gröbner et al., 2010). The analysis of erythemal UV doses at different sites in Austria and Switzerland also  
50 demonstrates a significant growth of UV radiation with the altitude (Rieder et al., 2010). In the Arctic the  
51 comparison of summer UV measurements at Summit (3202m a.s.l.) and Barrow (~0 a.s.l.) stations also shows  
52 significant enhancing of about 30-40% in clear sky conditions at the elevated site (Bernhard et al., 2008).

53 The UV altitude gradients obtained from model calculations vary within the range of 3.5-6%/km in the cloudless  
54 atmosphere if all other parameters (ozone, aerosol, surface albedo) do not change with the altitude (Chubarova and  
55 Zhdanova, 2013). Even smaller values of the estimated UV altitude gradients (3.5%/km) were obtained in conditions  
56 with high surface albedo at both sea level and high altitude, since the larger diffuse component at sea level, to some  
57 extent, compensates the higher direct flux due to a smaller total optical depth at higher altitudes. However, the  
58 experimental UV altitude gradients are often much higher due to the presence of additional altitude changes in the  
59 atmospheric parameters. According to different field campaigns UV altitude gradients vary within 5-11%/km  
60 (Pfeifer et al., 2006, Zaratti et al., 2003, Schmucki, Philipona, 2002), 11-14%/km according to (Sola et al., 2008),  
61 and in some cases can reach 31%/km (Pfeifer et al., 2006). The existence of spectral dependence in absorption  
62 coefficients of ozone as well as in molecular scattering cross sections provides a pronounced spectral character of  
63 the altitude UV effect, which was obtained in many publications (Blumthaler et al., 1994, Sola et al., 2008).

64 However, the continuous UV records in mountainous area are still very rare due to the complexity of accurate UV  
65 measurements in severe conditions. The accurate results of measurements from different field campaigns devoted to  
66 the evaluation of altitude UV effects shown in (Bernhard et al., 2008, Blumthaler and Ambach, 1988, Blumthaler et  
67 al., 1994, Blumthaler et al., 1997, Dahlback et al., 2007, Lenoble et al., 2004, Piacentini, et al. 2003, Pfeifer et al.,  
68 2006, Sola et al., 2008, Zaratti et al., 2003) provide precise, however, local character of this phenomenon, which  
69 results in various altitude UV gradients.

70 At the same time, the accurate RT (Radiative Transfer) model simulations (Liou, 2010) are very time consuming  
71 and can not be used in different on-line tools or other applications. There are also a lot of UV model assessments for  
72 the past and future UV climate scenarios but usually they are given with the coarse spatial resolution, which does  
73 not allow a user to obtain the accurate estimates over the particular mountainous location.

74 In addition, the limiting factor of the UV calculation accuracy is the uncertainty of input geophysical parameters,  
75 which significantly increases at high altitudes. Hence, another task was to obtain some generalized dependencies of  
76 the input parameters using the available data sources.



77 The objective of this paper is to provide the accurate parameterization for different types of biologically active  
78 radiation for the estimation of UV level at different altitudes taking into account the generalized altitude dependence  
79 of different geophysical parameters. Using the proposed parameterization we will also discuss the consequence of  
80 the enhanced UV level at high altitudes for human health using the classification of UV resources via a specially  
81 developed on-line interactive UV tool.

## 82 2. Materials and methods

83 In order to account for different effects of UV radiation on human health we analyze three types of BAUVR:  
84 erythemally-weighted, vitamin D-weighted, and cataract-weighted irradiances, which are calculated using the  
85 following equation:

$$86 \quad Q_{bio} = \int_{280}^{400} Q_{\lambda} F_{\lambda} d\lambda, \quad (1)$$

87 where  $Q_{\lambda}$  is the spectral flux density,  $F_{\lambda}$  is the respective biological action spectrum.

88 We used erythral action spectrum according to CIE (1998), vitamin D spectrum - according to CIE (2006), and  
89 cataract-weighted spectrum according to Oriowo et al. (2001). Various types of BAUVR action spectrum have  
90 different efficiency within the UV range. For their characterization we used the effective wavelengths, which are  
91 calculated as follows:

$$92 \quad \lambda_{eff} = \frac{\int Q_{\lambda} \lambda d\lambda}{\int Q_{\lambda} d\lambda} \quad (2)$$

93 According to our estimates, for example, at high solar elevation ( $h=60^{\circ}$ ) and for the variety of other parameters  
94 (total ozone, aerosol and surface albedo) the effective wavelength for erythemally-weighted irradiance ( $Q_{ery}$ ) is  
95  $\sim 317$  nm, for cataract-weighted irradiance ( $Q_{eye}$ ) -  $\sim 313$  nm, and for vitamin D-weighted irradiance ( $Q_{vitD}$ ) -  
96  $\sim 308$  nm. These changes in effective wavelengths for various BAUVR types indicate their different sensitivity to the  
97 ozone absorption, molecular scattering and aerosol attenuation, which vary dramatically within this spectral range,  
98 and, as a result, explain different BAUVR responses to the changes in these geophysical parameters.

99 All the simulations were fulfilled using one dimensional radiative TUV (Tropospheric Ultraviolet-Visible) model  
100 with 8-stream DISORT RT method (Madronich and Flocke, 1997) and 1 nm spectral resolution. The uncertainty of  
101 the RT method is less than 1% (Liou, 2010). Badosa et al.(2007) showed a good agreement between the  
102 experimental spectral data in different geographical regions and simulated results using this RT method if the input  
103 atmospheric parameters were known.

104 Several experimental datasets were used. For obtaining the generalized altitude dependence of aerosol optical depth  
105 (AOD) we used the data of sun/sky CIMEL photometers from different AERONET sites located at different heights  
106 above sea level (Holben et al., 1998)). These data account for the near-ground emission sources of the aerosol at  
107 various altitude in the aerosol column content. The estimated uncertainty for aerosol optical depth in UV spectral  
108 region is about 0.02. The uncertainty for single scattering albedo is about 0.03 at  $AOD_{440} > 0.4$  and the uncertainty  
109 for all other inversion parameters is not higher than 10% (Holben et al., 2006). In addition, the dataset of historical  
110 Moscow State University complex field campaigns over mountainous areas at Pamir (38- 40.5° N, 73-74° E  
111  $H=1.0\pm 3.9$  km), and Tyan'Shan' (43°N, 77°E,  $H=3.47$ km) was applied in the analysis (Belinski et al., 1968). It  
112  
113  
114  
115



116 includes the data records of total ozone content and aerosol optical depth at 330 nm, which had been measured with  
117 the help of M-83 filter ozonometer, and UV irradiance less 320 nm – by the UVM-5 instrument calibrated against  
118 the spectroradiometer BSQM (the Boyko’s Solar Quartz Monochromator) described in (Belinski et al., 1968). The  
119 description of the BSQM and the details of the calibration were also discussed in Chubarova and Nezval’ (2000).  
120 The uncertainties of UV measurements less 320nm due to the calibration procedure were considered to be about  
121 10% (Belinsky et al., 1968). However, to avoid the calibration errors only relative measurements were used in this  
122 study. The residual uncertainty due to possible existence of slight variation in spectral response of the instrument  
123 and their temperature dependence was estimated to be about 5-7%. The obscurity of the horizon at all sites was less  
124 than 10°. The field campaigns were carried out during summer periods, when no snow was detected at the surface.  
125 The snow covered mountainous peaks were only observed at Tyan’Shan’ at relatively large distance of more than 30  
126 km from the site.

127 We also used the LIVAS database (Lidar Climatology of Vertical Aerosol Structure for Space-Based Lidar  
128 Simulation Studies, <http://lidar.space.noa.gr:8080/livas/>). This is a 3-dimensional global aerosol climatology based  
129 on satellite lidar CALIPSO observations at 532 and 1064 nm, EARLINET ground-based measurements and a  
130 combination of input data from AERONET, aerosol models, etc. The final LIVAS climatology includes 4-year  
131 (2008 – 2011) time-averaged 1×1° global fields (Amiridis, et al., 2015). We used the annual aerosol extinction  
132 profiles at 355 nm for calculating aerosol optical depth over various points at different altitudes in the Alpine and  
133 the Caucasian mountainous regions in Europe and over the high-elevated regions in Asia. It should be mentioned  
134 that the LIVAS averages all Calipso overpasses over a 1x1° cell and characterizes only the mean altitude within the  
135 cell. This provides some additional uncertainties in its aerosol extinction altitude dependence evaluation. On  
136 average, according to (Amiridis et al., 2015) the absolute difference in LIVAS AOD is within 0.1 agreement with  
137 AERONET AOD values in UV and visible region of spectrum.

138 In addition, we estimated UV resources at different altitudes according to the approach given in Chubarova and  
139 Zhdanova (2013), which has been developed on the base of international classification of UV index (Vanichek et  
140 al., 2000) and the vitamin D threshold following the recommendations given in CIE (2006). According to this  
141 approach we defined *noon UV deficiency* and *100% UV deficiency categories*, when UV dose is smaller than the  
142 vitamin D threshold, and it is not possible to receive vitamin D respectively during solar noon hour, and throughout  
143 the whole day. The *UV optimum* category is determined when the UV dose does not exceed erythema threshold but  
144 it is possible to receive UV dose, necessary for vitamin D at noon hour. Several subclasses of *UV excess* are  
145 attributed to the thresholds depending on the standard UV index categories: *moderate UV excess* class, which relates  
146 to moderate category of hourly UV index, *high UV excess*, *very high UV excess*, and *extremely high UV excess*  
147 category. Currently, in the assessment of UV resources we do not take into account for the eye damage UV effects,  
148 since there is no reliable regulation on the UV threshold for this type of BAUVR.

### 149 3. Results

#### 150 3.1. The general description of the approach

151 It is widely known that “the solution of the radiative transfer equation is possible to derive by numerous solution  
152 methods and techniques” (Liou, 2010). However, the accurate RT methods usually require a lot of computer time  
153 and can not be used in several applications. The simulated intensity and UV flux density (or irradiance) has a  
154 complicated non-linear dependence on many geophysical parameters, however, our numerous simulations of UV



155 irradiance using the accurate 8-stream discrete ordinate RT method show that within a variety of geophysical  
 156 parameters one can obtain the parameterized altitude correction by taking into account for the quasi-independent  
 157 terms driven by different geophysical factors. Some of them are independent due to different vertical profiles (for  
 158 example, ozone maximum in the stratosphere compared with aerosol and molecular maximum in the troposphere).  
 159 Some of them are dependent (for example, surface albedo UV effects depend on molecular and aerosol loading),  
 160 but, as we show later, this factor can be also considered as a one joint term.

161 Using this assumption, we propose a parameterization, where biologically active UV irradiance at the altitude  $H$   
 162 ( $Q_{bio}(H)$ ) can be estimated from  $Q_{bio}$  at zero altitude ( $H=0$  km a.s.l.) with an independent account for the terms,  
 163 which are affected by different geophysical factors:

$$164 \quad Q_{bio}(M_H, X_H, AOD_H, S_H) = Q_{bio}(M_0, X_0, AOD_0, S_0) \cdot A_M A_X A_{AOD} A_{S(M, AOD, cloud)}, \quad (3)$$

165 where  $A_M$ ,  $A_X$ ,  $A_{AOD}$  are the UV amplifications, respectively, due to the altitude decrease in molecular number  
 166 density ( $M$ ), ozone ( $X$ ), and aerosol optical depth ( $AOD$ ).  $A_{S(M, AOD, cloud)}$  is the UV amplification due to the increase in  
 167 surface albedo  $S$ , which is typically observed with the altitude. This characteristic is also a function of a change in  
 168 molecular number density, aerosol and cloud characteristics with height due to the processes of multiple scattering.  
 169 Further, only the effects in the cloudless atmosphere are considered. The total UV amplification ( $A_{UV}$ ) with altitude  $H$   
 170 can be rewritten from Eq.(3) as:

$$171 \quad A_{UV} = A_M A_X A_{AOD} A_S = \frac{Q_{bio}(M_H, X_H, AOD_H, S_H)}{Q_{bio}(M_0, X_0, AOD_0, S_0)} \quad (4)$$

172 Let us consider separately the effects of different factors on UV irradiance at high altitudes. We specify them by  
 173 using the accurate RT model simulations, different empirical datasets or by applying the important characteristics  
 174 from different publications.

175 The possibility of this approach was tested directly by the accurate modelling for a variety of conditions at different  
 176 solar elevations. The model simulations were made for the altitude changes from zero to 5 km with the variations of  
 177 aerosol optical depth at 340nm within  $AOD_{340} \sim 0.0-0.4$ , variations in total ozone from 350 to 250 DU, and surface  
 178 albedo changes from zero to  $S=0.9$  at different altitudes. As the input aerosol parameters within UV spectral region  
 179 we used single scattering albedo  $SSA=0.96$ , factor of asymmetry  $g=0.72$ , and Angstrom exponent of  $\alpha=1.0$ , which  
 180 are close to the aerosol background characteristics in Europe (Chubarova, 2009). We compared the  $A_{UV}$  values  
 181 calculated as a multiplication composite of different separate parameters ( $A_M$ ,  $A_X$ ,  $A_{AOD}$ , and  $A_S$ ) according to Eq.(4)  
 182 with the  $A_{UV}$  values, which were estimated as a ratio of direct simulations of BAUVR at the altitude  $H=5$  km and at  
 183 zero ground level. The results of the comparisons are shown in Fig.1. One can see a good agreement between the  
 184  $A_{UV}$  values obtained using multiplication of  $A_M A_X A_{AOD} A_S$  and the  $A_{UV}$  values from direct estimations of BAUVR.  
 185 The correlation for all BAUVR types is higher than 0.99 with the mean relative difference of  $-1 \pm 3\%$  compared with  
 186 the exact model simulations with the same input parameters. The slight variations in aerosol parameters (within  
 187 10%) does not change the obtained results.

### 188 3.2. Molecular UV amplification with the altitude

189 A decrease of atmospheric pressure, or molecular number density, with the height is a well-known factor of UV  
 190 amplification. According to the 8-stream DISORT model simulations we found that the BAUVR dependence with  
 191 the altitude has a linear change in the molecular atmosphere, which is clearly seen in Fig.2. Hence, for its  
 192 characterization we can apply a simple gradient approach.



193 For evaluating the UV amplification due to molecular effects the following expression is used:

$$194 \quad A_M = \frac{Q_{bio}(M_H, X_0, AOD_0, S_0)}{Q_{bio}(M_0, X_0, AOD_0, S_0)} = 1 + 0.01 G_{bio, M}(S=0) \Delta H \quad (5)$$

195 where  $G_{bio, M}$  is the relative molecular gradient, in %/km,  $\Delta H$  is the difference in the altitudes, in km. Note, that all  
 196 other parameters do not change with the height.

197 The estimated relative molecular gradients for different types of BAUVR for various conditions are shown in Table  
 198 1. At solar elevation  $h=10^\circ$  there is a decrease in the  $G_{bio, M}$  for different BAUVR and, especially, for vitamin-D  
 199 irradiance due to its smaller effective wavelength and the effects of stronger ozone absorption, which is increased at  
 200 higher ozone content ( $X=500$  DU). However, for solar elevation higher than  $20^\circ$  the sensitivity of the  $G_{bio, M}$  values is  
 201 around 6-7%/km and does not significantly change with variations in  $h$  and  $X$ .

202 As an example, at the altitude of 5km and at high solar elevation the molecular UV amplification according to Eq.  
 203 (5) lies within ~1.26-1.38 depending on the type of BAUVR (see Table 1), which is in accordance with the accurate  
 204 model simulations. However, at  $h=10^\circ$  the UV amplification for erythemally-weighted and cataract-weighted  
 205 irradiances is about 1.18-1.23, while for vitamin D-weighted irradiance  $A_M$  is only 1.04-1.09 depending on ozone  
 206 content. The maximum UV amplification at the highest peak (m. Everest,  $H=8.848$  km) due to changes only in  
 207 molecular scattering reaches 1.53-1.68 at high solar elevation depending on the type of BAUVR.

### 208 3.3. Ozone UV amplification with the altitude

209 In order to account for the ozone decrease with the altitude we apply the existing linear dependence between UV  
 210 radiation and total ozone  $X$  in log-log scale. This approach was used in the definition of the Radiation Amplification  
 211 Factor (RAF) by Booth and Madronich (1994). As a result, the following equation can be written:

$$212 \quad \log(Q_{bio}) = RAF(Q_{bio, h}) \log(X_i) + C, \quad (6)$$

213 where  $h$  is the solar elevation,  $C$  is the constant.

214 The RAF values vary for different types of BAUVR. For example, at high solar elevation Radiation Amplification  
 215 Factor for erythemally-weighted irradiance  $RAF_{Q_{ery}} = 1.2$ , for vitamin D-weighted irradiance -  $RAF_{Q_{vitD}} = 1.4$ , for  
 216 cataract weighted irradiance -  $RAF_{Q_{eye}} = 1.1$  (UNEP, 2011). However, we should take into account the RAF  
 217 dependence on solar elevation  $h$  due to the relative changes in solar spectrum with  $h$ . Using the results of accurate  
 218 RT modelling we have obtained RAF dependencies on  $h$  for different types of BAUVR:

$$219 \quad RAF_{Q_{ery}}(h) = -1.10E-04 \pm 1.49E-5 h^2 + 1.57E-02 \pm 1.53E-3 h + 0.665 \pm 0.0333 \quad (7)$$

$$220 \quad R^2 = 0.98$$

$$221 \quad RAF_{Q_{vitD}}(h) = 0.000166 \pm 0.00001 h^2 - 0.0277 \pm 0.0011 h + 2.5121 \pm 0.0233 \quad (8)$$

$$222 \quad R^2 = 0.997$$

$$223 \quad RAF_{Q_{eye}}(h) = 1.43E-6 \pm 1.0E-6 h^3 - 0.000202 \pm 0.000066 h^2 + 0.00483 \pm 0.0029 h + 1.297 \pm 0.035 \quad (9)$$

$$224 \quad R^2 = 0.98$$

225 where  $R^2$  – is the determination coefficient. The standard error estimates of the coefficients in the equations are  
 226 given at P=95%.

227 Note, that similar approach for accounting the RAF solar angle dependence was proposed in Herman (2010) with  
 228 higher power degree.



229 As a result, the BAUVR at the altitude  $H(Q_{bioH})$  with the correction on ozone content can be written as follows:

$$230 \quad Q_{bioH} = Q_{bio0}(X_0/X_H)^{RAF(Q_{bio,h})} \quad (10)$$

231 From Eq.(10) we can obtain the altitude UV amplification due to ozone using the altitude ozone gradient  $G_X$   
232 (DU/km):

$$233 \quad A_X = \frac{Q_{bio}(M_0, X_H, AOD_0, A_0)}{Q_{bio}(M_0, X_0, AOD_0, A_0)} = \left( \frac{X_0}{X_0 - G_X \cdot \Delta H} \right)^{RAF(Q_{bio,h})} \quad (11)$$

234 We propose to apply the typical ozone altitude gradient  $G_X$ , which absolute value is about 3.5 DU/km according to  
235 monthly averaged ozone soundings measurements in Germany and observations in Bolivia (Reuder and Koepke,  
236 2005; Pfeifer et al., 2006).

237 As an example, if we take into account only for this typical ozone decrease with the altitude, the UV enhancement at  
238 5 km will be about  $A_X \sim 1.06-1.11$  while at the highest peak (m. Everest)  $A_X$  will reach 1.11-1.22 at high solar  
239 elevations depending on the BAUVR type and initial ozone content at zero altitude within  $X=250-350$  DU.

#### 240 **3.4. Aerosol UV amplification with the altitude**

241 Aerosols can significantly change their characteristics with the altitude, affecting the level of BAUVR. Due to  
242 variations in size distribution and optical properties aerosol may have different radiative properties (aerosol optical  
243 depth, single scattering albedo, and phase function). One of the most important aerosol characteristics affecting UV  
244 radiation is aerosol optical depth.

245 For accounting the aerosol effect on UV attenuation we propose to apply the equation given in (Chubarova, 2009):

$$246 \quad Q_{bio}(AOD_{340}) = Q_{bio}^*(AOD=0)(1 + AOD_{340} B) \quad (12)$$

247 where  $B = (0.42m + 0.93) SSA - (0.49m + 0.97)$ ,  $Q_{bio}^*$  is the BAUVR in aerosol free conditions,  $m$  is the air mass, SSA is  
248 the single scattering albedo.

249 The Eq. (12) was obtained from the accurate model simulations for the conditions with low surface albedo ( $S=0.02$ ),  
250 which is typical for grass. (Here and further we consider AOD at wavelength 340nm ( $AOD_{340}$ ), since this  
251 wavelength corresponds to the standard UV channel in CIMEL sun/sky photometer, which is used in AERONET).

252 The coefficients were obtained according to model simulations for  $0 < AOD_{340} < 0.8$ , single scattering albedo  
253 ( $0.8 < SSA < 1$ ), and air mass  $m \sim \sinh^{-1}(m \leq 2)$ , Angstrom exponent  $\alpha \sim 1$ . Since the radiative effects of the existing AOD  
254 spectral dependence are relatively small within the UV-B spectral range we consider the same coefficients for  
255 different types of BAUVR.

256 Assuming that single scattering albedo and factor of asymmetry do not change with the altitude, we evaluated the  
257 UV amplification with the altitude due to aerosol optical depth. Using Eq.(12) the equation for  $A_{AOD340}$  can be  
258 written as follows:

$$259 \quad A_{AOD340} = \frac{Q_{bio}(M_0, X_0, AOD_H, A_0)}{Q_{bio}(M_0, X_0, AOD_0, A_0)} = \frac{1 + AOD_{340,H} B}{1 + AOD_{340,0} B} \quad (13)$$

260 In some conditions single scattering albedo and asymmetry factor may have the altitude dependence (see, for  
261 example, the results of aircraft measurements in (Panchenko et al., 2012)). However, the uncertainty of neglecting  
262 the altitude changes in single scattering albedo significantly decreases at small AOD observed at high altitudes. We  
263 should also note that only the altitude changes in aerosol optical depth are usually taken into account in the standard  
264 tropospheric aerosol models (WMO, 1986).



265 The aerosol optical depth at the altitude  $H(AOD_{340,H})$  can be evaluated using the following expression:

$$266 \quad AOD_{340,H} = AOD_{340,0} f_{AOD}(H), \quad (14)$$

267 where  $f_{AOD}(H)$  is the altitude dependence of aerosol optical depth.

268 There are a lot of model aerosol profiles for the free atmosphere conditions (see, for example, widely used aerosol  
 269 models in WMO, (1986)). However, these profiles can not be applied for high-elevated locations, which are usually  
 270 characterized by a significant emission of primary aerosols or their precursors from nearby surface even in  
 271 background conditions. To account for this kind of altitude AOD dependence we used different ground-based and  
 272 satellite measurements described in the Section 2. Since our objective was to obtain the generalized aerosol altitude  
 273 dependencies we used the monthly mean AOD data from different archives over different geographical regions in  
 274 Eurasia. The dependence of aerosol optical depth as a function of altitude is shown in Fig.3. Highly variable  $AOD_{340}$   
 275 values at different altitudes may be roughly combined in two groups, which are characterized by different rates of  
 276 aerosol altitude decrease. Hence, in our parameterization we propose to distinguish these two types of the altitude  
 277 aerosol dependence. The first one is characterized by a very strong aerosol optical depth decrease with the altitude.  
 278 It was obtained mostly from the data of European AERONET sites in the Alpine zone as well as from several Asian  
 279 sites in the sharp-peak mountainous areas. This dependence was also confirmed by the LIVAS dataset  
 280 measurements over the same areas.

281 The second one is characterized by a much more gradual altitude  $AOD_{340}$  decrease observed over flat elevated Asian  
 282 regions. The main reason of such a character is the existence of the additional aerosol emission sources (i.e. loess,  
 283 mineral aerosol) from the vast areas of deserts and semi-deserts elevated over sea level of up to 3-4 kilometers.

284 In addition, Fig.3 demonstrates the  $AOD_{340}$  dependence on altitude according to the data obtained during Moscow  
 285 State University field campaigns at the high-altitude plateau at Pamir and Tyan'-Shan' mountainous regions in  
 286 Central Asia. We can see its satisfactory agreement with the second type of  $f_{AOD}(H)$  obtained from the AERONET  
 287 and LIVAS dataset.

288 The first, Alpine – like type, can be parameterized as:

$$289 \quad f_{AOD}(H) = H^{-1.65}, R^2 = 0.4 \quad (15)$$

290 The Alpine type aerosol altitude dependence was firstly obtained for the simulation of the UV climatology over  
 291 Europe (COST 726, 2010). However, the coefficients have been re-affirmed using more statistics.

292 The second, so-called Asian type, can be obtained using the equation according to the Moscow State University  
 293 expedition dataset in Asian region. It is characterized by much flat dependence with the altitude:

$$294 \quad f_{AOD}(H) = \exp(-0.26H), R^2 = 0.8 \quad (16)$$

295 The proposed dependencies can be considered as the two classes with different altitude aerosol decreasing rates.

296 Both dependencies are accounted for the altitudes higher than 1 km, since our analysis of AERONET dataset has  
 297 revealed the absence of the aerosol altitude dependence at the heights below 1 km due to prevailing the effects of  
 298 different aerosol sources or their precursors there. However, over the particular location the altitude AOD  
 299 dependence within the first kilometre can be found, of course.

300 We should note that the proposed altitude AOD dependencies according to (15) and (16) are considered only as a  
 301 first proxy for the most sharp and flat altitude dependencies. For a particular location and specific geographical  
 302 conditions the AOD altitude dependence can be different. However, a user may easily substitute them in the  
 303 proposed parameterization.



304 Although the  $AOD$  altitude dependence is pronounced, its influence on UV amplification highly depends on initial  
 305 aerosol conditions at  $H=0$  km, the type of the altitude profile, and solar elevation (see Eq. (12)). For example, for the  
 306 Alpine type aerosol altitude profile the UV amplification at  $H=5$  km is about  $A_{AOD}=1.05-1.10$  and does not exceed  
 307  $1.11$  at  $H=8.848$  km for typical aerosol at  $H=0$  km ( $AOD_{340}=0.36$ ). However, for the polluted conditions  
 308 characterized by  $AOD_{340}=0.8$  at  $H=0$  km, the altitude UV amplification at  $H=5$  km is about  $A_{AOD}\sim 1.12-1.27$   
 309 depending mainly on solar elevation. Note, that at  $H=8.848$  km the effect is almost the same ( $A_{AOD}\sim 1.16-1.29$ ). This  
 310 will be further discussed below.

### 311 3.5. UV amplification due to changes in surface albedo with the altitude

312 The increase in surface albedo is one of the important factors, which is necessary to account for the effective  
 313 calculations of BAUVR at high altitudes. Due to significant negative temperature gradients, the snow with high  
 314 surface albedo can be observed even in summer conditions at high altitudes instead of vegetation with low UV  
 315 albedo of about  $S=0.02-0.05$  (Feister and Grewe, 1995). Fig.4 demonstrates the enhancement in erythemally-  
 316 weighted irradiance due to the increase in surface albedo according to different experimental studies and the results  
 317 of one-dimensional model simulations. One can see the UV increase of around 20% at the effective surface albedo  
 318 close to  $S=0.5$  (Simic et al., 2011, Huber et al., 2004, Smolskaia et al., 2003). On the average, there is an agreement  
 319 between the calculation of UV amplification by 1D model and the measurements at different mountainous regions  
 320 up to effective surface albedo of  $S\sim 0.5$ . However, the accurate comparison of UV measurements with 3D model  
 321 (Diemoz and Mayer, 2007) shows the additional snow effect of about  $\pm 1$ UV index value due to the account of  
 322 overall interactions between radiation and different surfaces. The comparisons of UV spectral actinic flux  
 323 measurements with 1D and 3D model simulations demonstrate the similar range of uncertainties of these models,  
 324 however, 3D model gives, of course, more realistic view of the UV field in mountains since the topography and the  
 325 obstruction of the horizon are taken into account (Wagner et al., 2011). However, currently we do not consider 3D  
 326 effects in our parameterization. Due to small UV albedo over snow free surfaces this factor is negligible in summer,  
 327 while in winter the value of the effective surface albedo in mountainous area can be very high and significantly  
 328 depends on tree line location.

329 To account for surface albedo effects we followed the results obtained in different papers (Green, et al., 1980,  
 330 Chubarova, 1994), where the effects of multiple scattering were accounted using geometric progression approach.  
 331 The same approach with a detailed physical analysis was used in (Lenoble, 1998). Following these publications we  
 332 propose to calculate biologically active UV radiation in conditions with surface albedo  $S$  as follows:

$$333 \quad Q_{bio_S} = Q_{bio_{S=0}} \frac{1}{1-r_{bio}S} \quad (17)$$

334 where  $r_{bio}$  is the coefficient, which characterizes the maximum relative change in  $Q_{bio}$  due to multiple scattering for  
 335 surface albedo variations from 0 to 1. According to (Lenoble, 1998)  $r_{bio}$  is determined as the atmospheric reflectance  
 336 illuminated on its lower boundary. Note, that surface albedo  $S$  characterizes the reflecting properties at ground at the  
 337 considered altitude  $H$ .

338 The application of the equation (16) to  $H=0$  km and to the altitude  $H$  allows us to obtain the following expression  
 339 for  $Q_{bio}$  at  $H$  with surface albedo  $S_H$ : using the known  $Q_{bio}$  at the altitude  $H=0$  km with surface albedo  $S_0$ :

$$340 \quad Q_{bio_{S_H}}(H) = Q_{bio_{S_0}}(H=0) \frac{Q_{bio_{S=0}}(H) \cdot 1-r_{bio}(H=0)S_0}{Q_{bio_{S=0}}(H=0) \cdot 1-r_{bio}(H)S_H} \quad (18)$$

341 This equation can be rewritten in the following way:



$$342 \quad \frac{Q_{bioS_H}(H)}{Q_{bioS_0}(H=0)} = \frac{Q_{bioS=0}(H)}{Q_{bioS=0}(H=0)} \frac{1-r_{bio}(H=0)S_0}{1-r_{bio}(H)S_H} \quad (19)$$

343 One can see that in Eq. (19) the left side of the equation  $\frac{Q_{bioS_H}(H)}{Q_{bioS_0}(H=0)}$  is the total UV amplification  $A_{UV}$  defined in  
 344 equation (4); the first term  $(\frac{Q_{bioS=0}(H)}{Q_{bioS=0}(H=0)})$  at the right side of the equation characterizes the total UV amplification in  
 345 conditions with  $S=0$ , while surface albedo effects are accounted only in the last term. Hence, we can write the UV  
 346 amplification due to the effects of surface albedo as follows:

$$347 \quad A_S = \frac{1-r_{bio}(H=0)S_0}{1-r_{bio}(H)S_H} \quad (20)$$

348 According to the model estimations the value  $r_{bio}$  in clear sky conditions has a relatively small dependence on  
 349 altitude, which appears due to a decrease mainly in molecular and aerosol loading and can be easily parameterized  
 350 by a simple regression as follows:

$$351 \quad r_{bio}(H) = bH + c, \quad (21)$$

352 where the coefficients  $b$  and  $c$  are given in Table 2 for different types of BAUVR. They were obtained for a variety  
 353 of solar elevation and ozone content taking into account for the altitude changes in molecular scattering as well as  
 354 for altitude dependence of aerosol optical depth  $f_{AOD}(H)$ . The  $r_{bio}(H)$  mainly depends on molecular content and  
 355 aerosol properties, and slightly decreases with the altitude due to reducing in multiple scattering effects with the  
 356 decrease in molecular and aerosol loading.

357 As a result, the UV amplification due to the increase in surface albedo at the altitude  $H$  strongly depends on  
 358 scattering processes and also decreases with the altitude. Fig.5 shows the maximum  $A_S$  effect due to the changes in  $S$   
 359 from  $S=0$  at zero level to  $S=1$  at the altitude  $H$  for the different types of BAUVR. The  $A_S$  decreases with the altitude  
 360 from more than 1.6 at  $H=0$  km to about 1.2 at  $H=8.848$  km due to the decrease in  $r_{bio}$ .

### 361 3.6. Validation

362 Using the generalized parameterizations for different geophysical parameters obtained in the previous sections we  
 363 can estimate the total UV amplification  $A_{UV}$  with the altitude from Eq.(4). The results of the validation of the  
 364 proposed method with these altitude parameter dependencies against the accurate RT simulations are shown in  
 365 Fig.6. One can see a close correlation ( $r>0.996$ ) between the  $A_{UV}$  values obtained by the proposed method and the  
 366 accurate RT simulations using the 8-stream DISORT method within the changes in altitude from  $H=0$  km to 8 km,  
 367 in solar elevation from 20 to 50°, in surface albedo from  $S=0$  to  $S=0.9$ , in ozone from 250 DU to 350 DU at  $H=0$  km,  
 368 and in  $AOD_{340}$  from 0.2 to 0.4 at  $H=0$  km. Different altitude aerosol profiles were also considered. Validation was  
 369 made for all three types of BAUVR. Overall, the average bias is  $0\pm 0.2\%$  for erythemally-weighted irradiance, and  
 370  $1\pm 0.2\%$  - for other types of BAUVR. The maximum difference between the  $A_{UV}$  calculated by the proposed method  
 371 and by the accurate model simulations does not exceed 6% at the highest elevation ( $H=8$  km) at low ozone content.  
 372 The comparisons of the total UV amplification according to the proposed method with the total  $A_{UV}$  obtained from  
 373 the experimental dataset as a function of altitude are shown in Fig.7. The experimental data were taken from the  
 374 dataset of Moscow State University mountainous field campaigns, which was described in the Section 2. After  
 375 accounting for the molecular, aerosol, and ozone altitude dependence the simulated UV amplification is in  
 376 satisfactory agreement with the obtained experimental results.

377 **4. Discussion**

378 The total altitude amplification of biologically active UV irradiance  $A_{UV}$  as a function of altitude is shown in Fig.8  
379 for a variety of atmospheric conditions at surface albedo  $S=0$  and  $S=0.9$  and high solar elevation  $h=50^\circ$ . One can see  
380 a distinct altitude difference obtained for different types of BAUVR with larger increase for vitamin D-weighted  
381 irradiance due to its higher sensitivity to ozone content. The difference in  $A_{UV}$  for various BAUVR can reach 15-  
382 20% at high altitudes. The effects of surface albedo on  $A_{UV}$  can be seen if compare the results shown in Fig 7a and  
383 Fig.8b. One can see the 2-2.5 times UV increase due to high surface albedo at high altitudes, which is again more  
384 pronounced for vitamin D-weighted radiation with smaller effective wavelength and, hence, more effective multiple  
385 scattering than that for the other types of BAUVR. Larger  $A_{UV}$  values are also observed in conditions with smaller  
386 ozone amount for all three types of BAUVR for both zero and high surface albedo conditions. High surface albedo  
387  $S=0.9$  provides a significant increase even at zero level, which is similar to the  $A_{UV}$  increase due to altitude change  
388 of 6 km. It is clearly seen that typical aerosol and ozone does not play a vital role in  $A_{UV}$ . However, for all types of  
389 BAUVR the increase of slightly absorbing aerosol (from  $AOD_{340}=0.2$  to  $AOD_{340}=0.4$ ) provides a noticeable  $A_{UV}$   
390 growth in conditions with relatively small ozone content due to enhancement of multiple scattering (see Fig.8).

391 The  $A_{UV}$  values are smaller at solar elevation  $h<20^\circ$  for all types of BAUVR mainly due to decreasing in  $G_{bio,M}$  (see  
392 the coefficients in Table 1). For example, at  $H=8$  km the UV altitude amplification for vitamin D-weighted radiation  
393 is about  $A_{UV}=1.77$  at  $h=10^\circ$  compared with  $A_{UV}=2.0$  at  $h=50^\circ$  at  $X=250$  DU and  $AOD_{340}=0.4$ .

394 Let us consider the conditions, which are characterized by the most pronounced UV amplification with the altitude -  
395 the conditions with high aerosol loading  $AOD_{340}=0.8$ , low ozone content  $X=250$ DU at  $H=0$  km, and high solar  
396 elevation  $h=50^\circ$ . In addition, we consider the abrupt increase in surface albedo at  $H=2$  km from  $S=0$  to  $S=0.95$ ,  
397 which can be possible due to location of tree line there and pure snow above. The altitude UV amplification due to  
398 these input parameters according to the proposed  $A_{UV}$  parameterization is shown in Fig.9. The separate effects of  
399 different factors can be seen in Fig. 9a and their total effects on different BAUVR types are shown in Fig.9b. One  
400 can see a different role of geophysical factors at different altitudes: the prevalence of molecular scattering especially  
401 at high altitudes while the extremely high surface albedo may play the most important role at the altitudes of its  
402 abrupt increase (in our case -  $H=2$ km,  $A_S=1.48$ ). However, in our example the UV amplification due to surface  
403 albedo decreases at the altitude higher than 2 km because of the reduction in multiple scattering. The UV altitude  
404 amplification due to aerosol is more distinct and reaches 1.1-1.2 at high altitudes if there is a strong aerosol pollution  
405  $AOD_{340}=0.8$  at  $H=0$  km. It is more pronounced for the Alpine-type AOD altitude dependence and in our example at  
406  $H=2$  km it can be even higher than the  $A_M$  value (see Fig.9). The effects of ozone in UV amplification do not exceed  
407 1.1-1.20 at high altitudes depending on BAUVR type. We would like to emphasize that Fig.9 is only the illustration  
408 of the application of the proposed  $A_{UV}$  parameterization for a given parameters altitude variations.

409 We implemented the proposed UV altitude parameterization in the developed on-line UV tool <http://momsu.ru/uv/>,  
410 which had been developed for the simulation of erythemally-weighted irradiance and the UV resources over  
411 Northern Eurasia (the PEEEX domain) at  $H=0$  km (Chubarova and Zhdanova, 2013). Using this program it is  
412 possible to calculate UV irradiance and UV-resources for different atmospheric conditions at a given geographic  
413 location and specified time. Based on the threshold for vitamin D and erythemally active irradiance the UV  
414 resources are obtained for various skin types and open body fraction. According to the classification we consider  
415 different categories of UV-deficiency, UV-optimum and UV-excess (Chubarova and Zhdanova, 2013). The  
416 interactive on-line UV tool represents a client-server application where the client part of the program is the web-  
417 page with a special form for the input parameters required for erythemally-weighted UV irradiance simulations. The



418 server part of the program consists of the web-server and the CGI-script, where the different input parameters are set  
419 by a user or taken from the climatological data available at the same site. In addition, in this part of the program  
420 erythemally-weighted irradiance is calculated, visualized and classified according to the proposed UV resources  
421 categories. The proposed UV irradiance altitude parameterization has been also incorporated in the calculation  
422 scheme with additional account for the changes in the atmospheric parameters with the height. This enable a user to  
423 evaluate UV irradiance at any requested elevation above sea level taking into account for a variety of the altitude  
424 dependent parameters.

425 Let us analyze the UV resources for skin type 2 and the open body fraction of 0.25 in the Alpine region  
426 (approximately 46°N and 7°E) for winter and spring noon conditions. On January, 15<sup>th</sup>, the noon UV deficiency (no  
427 vitamin D generation) conditions (with noon erythemally UV dose of about 97.2 Jm<sup>-2</sup>) are observed at  $H=0$  km for  
428 typical (climatological) ozone, aerosol and surface albedo conditions, while at the same location the UV optimum is  
429 observed at  $H$  higher 0.5 km up to  $H=4.807$  km (the highest point within the Alps, peak Mont Blanc) with noon  
430 erythemally UV dose variation from 100.6 Jm<sup>-2</sup> to 122.9 Jm<sup>-2</sup>. However, for skin type 4 according to the skin type  
431 classification (Fitspatrick, 1988) the noon UV deficiency is observed at all altitudes and even at high surface albedo  
432  $S=0.9$  corresponding to the pure snow with UV dose of 154.4 Jm<sup>-2</sup>. If we increase the open body fraction for skin  
433 type 4 from 0.25 to 0.5 the vitamin D generation is possible and, hence, the conditions are classified as UV  
434 optimum.

435 On April, 15<sup>th</sup> for open body fraction 0.25 and typical climatological conditions at this geographical point the  
436 moderate UV excess is observed for skin type 2, and the UV optimum - for skin type 4 at  $H=0$  km with noon UV  
437 dose of about 437.7 Jm<sup>-2</sup>. At the altitude  $H = 2$  km the conditions are characterized by the moderate UV excess for  
438 skin type 2 and, still, by the UV optimum - for skin type 4 with UV dose of 463.4 Jm<sup>-2</sup>. At the  $H=4$  km a high UV  
439 excess is observed for skin type 2 and the moderate UV excess - for skin type 4 with UV dose of 532.4 Jm<sup>-2</sup>.

440 Thus, the proposed altitude UV parameterization can be effectively used for accurate estimating the BAUVR at  
441 different altitudes with any altitude resolution for a variety of geophysical parameters over the PEEX domain in  
442 Northern Eurasia. The accurate RT methods like Monte-Carlo, Discrete Ordinate method or others, of course, can be  
443 used instead for UV irradiance simulations, however, their application is very time-consuming and are not possible  
444 in some applications. The proposed approach is especially very useful for the application in different kinds of on-  
445 line UV tools, where it is not possible to use a lot of prescribed calculations for a wide set of different geophysical  
446 parameters or accurate UV modelling.

447 The combination of different altitude dependencies for main geophysical factors in the proposed parameterization  
448 allows a user to make a reliable altitude UV assessment. It is not, of course, possible to take into account for the  
449 specific altitude dependencies. We should also emphasize that the proposed ozone and aerosol altitude dependencies  
450 in the troposphere were taken from the experimental data obtained in background conditions and, hence, should be  
451 applied only for these conditions. However, they can be easily substituted using the proposed parameterization.

452 With the application of the proposed method we can also reveal the effects of different geophysical factors on  
453 various types of BAUVR and estimate their comparative role in the altitude UV effects. And, of course, it can be  
454 also used in downscaling the UV results for the regions located at high altitudes from the coarse resolution global  
455 chemistry-climate models. The proposed method can be applied not only over the PEEX domain but on a global  
456 scale over the world. However, more attention should be paid in this case to the evaluation of the particular altitude  
457 dependence of the different parameters.



## 458 5. Conclusions

459 The objective of this paper was to develop a flexible parameterization based on rigorous model simulations with  
460 account for generalized altitude dependencies of molecular density, ozone, and aerosols considering surface albedo  
461 conditions. We show that for the specified groups of parameters we can present the altitude UV amplification ( $A_{UV}$ )  
462 for different BAUVR as a composite of independent contributions of UV amplification from different factors with  
463 the mean uncertainty of 1% and standard deviation of 3%. The parameterization takes into account for the altitude  
464 dependence of molecular number density, ozone content, aerosol loading, and spatial surface albedo. We also  
465 provide the generalized altitude dependencies of different parameters for evaluating the  $A_{UV}$ . Their validation against  
466 the accurate RT model (8 stream DISORT RT code) for different types of BAUVR shows a good agreement with  
467 maximum uncertainty of few percents and correlation coefficient  $r > 0.996$ . It was not possible, of course, to cover  
468 all the observed variety in the parameters. However, due to the proposed approach the parameter altitude  
469 dependencies can be easily substituted by a user.

470 Using this parameterization one can estimate the role of different atmospheric factors in the altitude UV variation.  
471 The decrease in molecular number density, especially at high altitudes, and the increase in surface albedo play the  
472 most significant role in  $A_{UV}$  growth. At high solar elevations the UV amplification due to aerosol at  $H=8.848$  km  
473 does not exceed 1.3 even when  $AOD_{340}=0.8$  at  $H=0$  km. The UV amplification due to aerosol calculated with the  
474 Alpine-type AOD altitude aerosol dependence is much more pronounced than that calculated with the Asian-type  
475 AOD altitude dependence, especially at relatively lower altitudes ( $H=2-4$  km). The UV amplification due to ozone  
476 does not exceed 1.20 and is higher at smaller solar elevations, especially, for vitamin-D-weighted irradiance.

477 This parameterization was applied to the on-line tool for calculating the UV resources (<http://momsu.ru/uv/>) over the  
478 PEEEX domain. Using this tool one can easily evaluate the UV conditions (UV deficiency, UV optimum or UV  
479 excess) at different altitudes for a given skin type and open body fraction. As an example, we analyzed the altitude  
480 UV increase and its possible effects on health considering different skin types and various open body fraction for  
481 January and April conditions in the Alpine region. We showed that even in clear sky conditions over the same  
482 geographical point (46°N, 7°E) in mid-January the UV optimum can be observed higher  $H=0.5$  km for skin type 2  
483 while the UV deficiency are still remained at the altitudes up to  $H=4.8$  km for skin type 4. In mid-April the account  
484 for the altitude dependence at 4 km provides the changes from UV-optimum to UV excess for people with 4 skin  
485 type, and from moderate UV excess to the high UV excess conditions - for people with 2 skin type.

486 This approach can be also used in downscaling the results of global chemistry-climate models with the coarse spatial  
487 resolution in mountainous domain and as a simple tool for different types of applications for personal purposes of  
488 users.

## 489 Acknowledgements

490 The work was partially supported by the RFBR grant № 15-05-03612. We would like to thank all AERONET site  
491 PI's which data were used for obtaining the aerosol altitude dependence. We also are grateful to the LIVAS team for  
492 providing the aerosol extinction climatology.

## 493 References

494 Amiridis, V., Marinou, E., Tsekeri, A., Wandinger, U., Schwarz, A., Giannakaki, E., Mamouri, R., Kokkalis, P.,  
495 Biniotoglou, I., Solomos, S., Herekakis, T., Kazadzis, S., Gerasopoulos, E., Balis, D., Papayannis, A., Kontoes, C.,



- 496 Kourtidis, K., Papagiannopoulos, N., Mona, L., Pappalardo, G., Le Rille, O. and Ansmann, A.: LIVAS: a 3-D  
497 multi-wavelength aerosol/cloud climatology based on CALIPSO and EARLINET. *Atmos. Chem. Phys.*, 15, 7127-  
498 7153, 2015.
- 499 Badosa, J., McKenzie, R.L., Kotkamp, M. Calbo, J., Gonz'alez, J.A., Johnston, P.V., O'Neill, M. Anderson D.J.:  
500 Towards closure between measured and modelled UV under clear skies at four diverse sites. *Atmos. Chem. Phys.*,  
501 7, 2817–2837, 2007.
- 502 Bais, A.F., Lubin, D., Arola, A., Bernhard, G., Blumthaler, M., Chubarova, N., Erlick, C., Gies, H.P., Krotkov, N.,  
503 Mayer, B., McKenzie, R.L., Piacentini, R., Seckmeyer, G., Slusser, J.R.: Surface Ultraviolet Radiation: Past,  
504 Present, and Future, in: *Scientific Assessment of Ozone Depletion: 2006, Global Ozone Research and Monitoring*  
505 *Project—Report No. 50*. World Meteorological Organization, Geneva, Switzerland. Chapter 7, 2007.
- 506 Bekki, S., Bodeker, G. E., Bais, A. F., Butchart, N., Eyring, V., Fahey, D. W., Kinnison, D. E., Langematz, U.,  
507 Mayer, B., Portmann, R. W., Rozanov, E., Braesicke, P., Charlton-Perez, A. J., Chubarova, N. E., Cionni, I., Diaz,  
508 S. B., Gillett, N. P., Giorgetta, M. A., Komala, N., Lefèvre, F., McLandress, C., Perlwitz, J., Peter, T., and Shibata,  
509 K.: Future Ozone and Its Impact on Surface UV, in *Scientific Assessment of ozone Depletion: 2010, Global Ozone*  
510 *Research and Monitoring Project—Report 52*, World Meteorological Organization, Geneva, Switzerland. Chapter 3.  
511 2011.
- 512 Belinsky, V.A., Garadzha, M. P., Mezhenyaya, L. M. and Nezval', Ye. I.: *The Ultraviolet Radiation of Sun and Sky*  
513 (in Russian), ed. Belinsky V.A. Moscow State Univ. Press. Moscow, 1968.
- 514 Bernhard G., Booth, C. R. and Ehranjian, J. C.: Comparison of UV irradiance measurements at Summit,  
515 Greenland; Barrow, Alaska; and South Pole, Antarctica. *Atmos. Chem. Phys.*, 8, 4799–4810, 2008.
- 516 Blumthaler M., Ambach W.: Human solar ultraviolet radiant exposure in high mountains.  
517 *Atmospheric Environment*, 22, 4, 749-753, 1988.
- 518 Blumthaler, M., A. R. Webb, G. Seckmeyer, A. F. Bais, M. Huber, Mayer B.: Simultaneous spectroradiometry: A  
519 study of solar UV irradiance at two altitudes, *Geophys. Res. Lett.*, 21, 2805–2808, doi:10.1029/94GL02786, 1994.
- 520 Blumthaler, M., Ambach, W., Ellinger, R.: Increase in the UV radiation with altitude, *J. Photochem. Photobiol. B*,  
521 39, 130–134, 1997.
- 522 Booth, C. R., Madronich S.: Radiation amplification factors: Improved formulation accounts for large increases in  
523 ultraviolet radiation associated with Antarctic ozone depletion, in *Ultraviolet Radiation in Antarctica:*  
524 *Measurements and Biological Effects*, *Antarct. Res. Ser.*, 62, edited by C. S. Weiler and P. A. Penhale, AGU,  
525 Washington, D. C., 39-42, 1994.
- 526 Chubarova, N.Ye.: The transmittance of the Global Ultraviolet Radiation by Different Cloud Types. *Physics of the*  
527 *atmosphere and ocean*, English translation, 29 (5), 615-621, 1994.
- 528 Chubarova, N., Nezval', Ye.: Thirty year variability of UV irradiance in Moscow, *Journal of the Geophysical*  
529 *Research: Atmospheres*, 105, D10, 12529-12539, 2000.
- 530 Chubarova, N.Y.: Seasonal distribution of aerosol properties over Europe and their impact on UV irradiance.  
531 *Atmospheric Measurement Techniques*, 2, 593-608, 2009.
- 532 Chubarova, N., Zhdanova, Ye.: Ultraviolet resources over Northern Eurasia, *Journal of Photochemistry and*  
533 *Photobiology B: Biology*, Elsevier, 127, 38-51, 2013.
- 534 CIE, Erythema reference action spectrum and standard erythema dose. Rep., CIE Standrad Bureau, Vienna, Austria,  
535 4 pp, 1998.
- 536 CIE, Action Spectrum for the Production of Previtamin D3 in Human Skin. Vienna, Austria, 16 pp., 2006.



- 537 COST 726 (European Cooperation in Science and Technology), Final report of COST action 726 – Long Term  
538 Changes and Climatology of UV Radiation over Europe, edited by Z. Lityńska, P. Koepke, H. De Backer, J. Gröbner,  
539 A. Schmalwieser, and L. Vuilleumier, COST Earth System Science and Environmental Management, Luxembourg:  
540 Office for Official Publications of the European Communities, 137 pp. Available at: <http://www.cost726.org/>, 2010.  
541 Dahlback, A., Gelsor N., Stamnes J. J., Gjessing Y.: UV measurements in the 3000–5000 m altitude region in Tibet,  
542 J. Geophys. Res., 112, D09308, doi:10.1029/2006JD007700, 2007.  
543 Diémoz, H., Mayer, B.: UV radiation in a mountainous terrain: comparison of accurate 3D and fast 1D calculations  
544 in terms of UV index . In "One Century of UV Radiation Research" , 18-20 September 2007, Davos, Switzerland,  
545 Ed. J. Gröbner, Davos, Switzerland, 165-166, 2007.  
546 Feister, U., Grewe, R.: Spectral albedo measurements in the UV and visible region over different types of surfaces.  
547 J. Photochemistry and Photobiology, 62 (4), 736-744, 1995.  
548 Fitzpatrick, T.B.: The validity and practicality of sun-reactive skin types I through VI, Arch. Dermatol., 124, 869–  
549 871, 1988.  
550 Green, A.E.S., Cross, K. R. and Smith, L.: A. Improved analytic characterization of ultraviolet skylight.  
551 Photochemistry and Photobiology, 31 (1), 59–65, 1980.  
552 Herman, J. R.: Global increase in UV irradiance during the past 30 years (1979–2008) estimated from satellite data,  
553 J. Geophys. Res., 115, D04203, doi:10.1029/2009JD012219, 2010.  
554 Holben, B. N., Eck, T. F., Slutsker, I., Tanre, D., Buis, J. P., Setzer, A., Vermote, E., Reagan, J. A., Kaufman, Y. J.,  
555 Nakajima, T., Lavenu, F., Jankowiak, I., Smirnov, A.: AERONET - A federated instrument network and data  
556 archive for aerosol characterization, Rem. Sens. Environ., 66, 1-16, 1998.  
557 Holben, B. N., Eck, T., Slutsker, I., Smirnov, A., Sinyuk, A., Schafer, J., Giles, D., and Dubovik, O.: AERONET  
558 Version 2.0 quality assurance criteria, in: Remote Sensing of the Atmosphere and Clouds. Eds. Tsay, S.-C.,  
559 Nakajima, T., Singh, R. P., and Sridharan, R., Proc. of SPIE, Goa, India, 13–17 November, 6408, 2006.  
560 Huber, M., Blumthaler, M., Schreder, J., Schallhart, B., Lenoble, J.: Effect of inhomogeneous surface albedo on  
561 diffuse UV sky radiance at a high-altitude site, J. Geophys. Res., 109, D08107, doi: 10.1029/2003JD004113, 2004.  
562 Hülsen, G.: UV measurements at mountain sites. PMOD WRC Annual report 2012, p.36. Available at:  
563 [http://www.pmodwrc.ch/annual\\_report/annualreport2012.pdf](http://www.pmodwrc.ch/annual_report/annualreport2012.pdf), 2012.  
564 Gröbner J., G. Hülsen, Blumthaler, M.: Effect of snow albedo and topography on UV radiation. The proceedings of  
565 2010 UV workshop, New Zealand, Available at:  
566 [http://www.niwa.co.nz/sites/niwa.co.nz/files/effect\\_of\\_snow\\_albedo\\_and\\_topography.pdf](http://www.niwa.co.nz/sites/niwa.co.nz/files/effect_of_snow_albedo_and_topography.pdf), 2010.  
567 Lenoble, J.: Modeling of the influence of snow reflectance on ultraviolet irradiance for cloudless sky. Applied  
568 Optics. 37(12), p. 2441-2447, 1998.  
569 Lenoble, J., Kylling, A., Smolkaia, I.: Impact of snow cover and topography on ultraviolet irradiance at the Alpine  
570 station of Briançon. J. Geophys. Res. 109, D16209, 2004.  
571 Liou, K.N.: An Introduction to Atmospheric Radiation. International Geophysics Series. Academic press, 84, 2010.  
572 Madronich, S., Flocke, S.: Theoretical estimation of biologically effective UV radiation at the Earth's surface, in  
573 Solar Ultraviolet Radiation – Modeling, Measurements and Effects (Zerefos, C., ed). NATO ASI Series Vol.152,  
574 Springer-Verlag, Berlin, 1997.  
575 Oriowo, O.M., Cullen, A.P., Chou, B.R., Sivak, J.G.: Action spectrum for in vitro UV-induced cataract using whole  
576 lenses. Invest. Ophthalmol. & Vis. Sci. 42, 2596-2602, 2001.



- 577 Panchenko, M.V., Zhuravleva, T. B., Terpugova, S. A., Polkin, V.V., and Kozlov, V. S.: An empirical model of  
578 optical and radiative characteristics of the tropospheric aerosol over West Siberia in summer, Atmos. Meas. Tech.,  
579 5, 1513-1527, doi:10.5194/amt-5-1513-2012, 2012.
- 580 Pfeifer, M., Koepke, T., P., Reuder, J.: Effects of altitude and aerosol on UV radiation, J. Geophys. Res., 111,  
581 D01203, doi:10.1029/2005JD006444, 2006.
- 582 Piacentini, R.D., Cede, A., Bárcena, H.: Extreme solar total and UV irradiances due to cloud effect measured near  
583 the summer solstice at the high-altitude desertic plateau Puna of Atacama (Argentina), J. Atmos. Solar Terr. Phys.,  
584 65 (6), 727-731, 2003.
- 585 Reuder, J., Koepke, P.: Reconstruction of UV radiation over southern Germany for the past decades, Meteorol. Z.,  
586 14(2), 237–246.,2005.
- 587 Reuder, J., Ghezzi, F., Palenque, E., Torrez, R., Andrade, M., Zaratti, F.: Investigations of the effect of high surface  
588 albedo on erythemally effective UV irradiance: results of a campaign at the Salar de Uyuni. Bolivia J.  
589 Photochemistry PhotobiologyB: Biology, 87(1), 1-8, 2007.
- 590 Rieder, H. E., Staehelin, J., Weihs, P., Vuilleumier, L., Maeder, J. A., Holawe, F., Blumthaler, M., Lindfors, A.,  
591 Peter, T., Simic, S., Spichtinger, P., Wagner, J.E., Walker, D., Ribatet, M.: Relationship between high daily  
592 erythemal UV doses, total ozone, surface albedo and cloudiness: An analysis of 30 years of data from Switzerland  
593 and Austria. Atmospheric Research, 98(1), 9-20, 2010.
- 594 Schmucki, D.A., Philipona, R.: Ultraviolet radiation in the Alps: the altitude effect, Opt. Eng., 41 (12), 3090-3095,  
595 2002.
- 596 Simic, S., Fitzka, M., Schmalwieser, A., Weihs, P., Hadzimustafic, J.: Factors affecting UV irradiance at selected  
597 wavelengths at HoherSonnblick, Atmospheric Research, 101(4), 869–878, 2011.
- 598 Smolskaia, I., Masserot, D., Lenoble, J., Brogniez, C., de la Casinière A.: Retrieval of the ultraviolet effective snow  
599 albedo during 1998 winter campaign in the French Alps. Appl. Opt., 42(9), 1583-1587, 2003.
- 600 Sola, Y., Lorente J., Campmany E., de Cabo X., Bech J., Redano A., Martínez-Lozano J. A., Utrillas M. P.,  
601 Alados-Arboledas L., Olmo F. J., Dí'az J. P., Expo'sito F. J., Cachorro V., Sorribas M., Labajo A., Vilaplana J. M.,  
602 Silva A. M, Badosa J.: Altitude effect in UV radiation during the Evaluation of the Effects of Elevation and  
603 Aerosols on the Ultraviolet Radiation 2002 (VELETA-2002) field campaign, J. Geophys. Res., 113, D23202,  
604 doi:10.1029/2007JD009742, 2008.
- 605 Vanicek K., Frei, T., Litynska, Z., Shmalwieser, A.: UV-Index for the Public, COST-713 Action, Brussels, 27pp.,  
606 2000.
- 607 UNEP (United Nations Environment Programme), Environmental Effects of Ozone Depletion, 1998  
608 Assessment, Journal of Photochemistry and Photobiology B: Biology, 46, Published by Elsevier Science, 1-4,  
609 Published by Elsevier Science, 1998.
- 610 UNEP (United Nations Environment Programme) Environmental effects of ozone depletion and its interactions  
611 with climate change, Assessment, 2010, Journal of Photochemistry and Photobiology Sciences, 10, Published by  
612 Elsevier Science, 2011.
- 613 Wagner, J. E., Angelini, F., Blumthaler, M., Fitzka, M., Gobbi, G. P., Kift, R., Kreuter, A., Rieder, H.E., Simic, S.,  
614 Webb, A., Weihs, P.: Investigation of the 3-D actinic flux field in mountainous terrain. Atmospheric  
615 Research, 102(3), 300-310, 2011.
- 616 WMO, Radiation Commission, A preliminary cloudless standard atmosphere for radiation computations, WCP-112,  
617 WMO/TD-24, 53 pp., World Clim. Res. Programme, Int. Assoc. for Meteorol. and Atmos. Phys., Geneva, 1986.



618 Zaratti, F., Forno, R.N., Fuentes, J. G., Andrade, M.F.: Erythemally weighted UV variations at two high-altitude  
619 locations, *J. Geophys. Res.*, 108 (D9), 4623, 2003.  
620  
621

622 **FIGURE CAPTIONS**

623

624 Fig.1. The comparison of  $A_{UV}$  amplification factor calculated from Eq.(4) as multiplication of  $A_M A_X A_{AOD} A_S$  with  
 625 the direct model simulation of UV amplification. All the parameters ( $A_{UV}, A_M A_X A_{AOD} A_S$ ) were obtained from  
 626 accurate model simulations.

627 Comment. The simulations were performed for different altitudes ( $H=0$  and  $H=5\text{km}$ ), aerosol optical depth  
 628 ( $AOD_{340}= 0, 0.2, 0.4$ ), total ozone ( $X=250,300,350$  DU), surface albedo ( $S=0, S=0.9$ ) and solar elevations ( $h=20^\circ$   
 629 and  $50^\circ$ ). For estimating the UV amplification we assume at  $H=0$  km the conditions with  $350\text{DU}$ ,  $AOD_{340}=0.4$ ,  
 630  $S=0\%$  and normalized the BAUVR at the altitude  $H=5\text{km}$  to the value calculated with these parameters.

631 Fig.2. UV amplification due to decrease in molecular number density with the altitude  $H$  according to accurate  
 632 model simulations: TUV, 8- stream DISORT TUV model.  $h=50^\circ$ .  $X=300$  DU.

633 Fig.3. The altitude dependence of aerosol optical depth at 340nm with 1 sigma error bar according to the  
 634 AERONET, LIVAS and the Moscow State University datasets over European and Asian regions. May-September  
 635 period. The AOD at 330 nm the Moscow State University dataset and the AOD at 355nm from the LIVAS datasets  
 636 were recalculated to AOD at  $\lambda=340$  nm using the Angstrom parameter  $\alpha=1.3$ . See further details in the text.

637 Fig.4. UV amplification due to the surface albedo increase in mountainous areas according to different experimental  
 638 data and model simulations. The error bars of model simulation relates to the different input parameters – altitude of  
 639 2 and 3 km, solar elevation of 10, 30 and  $50^\circ$ , total ozone  $X=350\text{DU}$ ,  $AOD_{340}=0.17$  at  $P=95\%$ .

640 Fig. 5. The dependence of  $r_{bio}$  with the altitude for different BAUVR from accurate model simulations for a variety  
 641 of geophysical parameters (left axis) and maximum  $A_S$  effects due to changes in surface albedo from  $S=0$  at  $H=0$   
 642 km to  $S=1$  at level  $H$  (right axis). The  $r_{bio}$  regressions are shown in dashed line. Note, that the regression line for  
 643  $r_{Q_{eve}}(H)$  is the same as for  $r_{Q_{ery}}(H)$ . The coefficients of the regression equations and the ranges of the input  
 644 parameters at  $H=0$  are given in Table 2.

645 Fig.6. The comparison between the total altitude UV amplification according to the proposed method and the  $A_{UV}$   
 646 values evaluated using the accurate RT model (TUV, 8-stream DISORT method).

647 Fig.7. The comparison between the simulated UV amplification according to the proposed parameterization and the  
 648 UV amplification from the experimental data as a function of altitude. Moscow State University dataset. Solar  
 649 elevation  $h=50^\circ$ . Clear sky conditions. Note: since we used the data of different field campaigns the ozone altitude  
 650 gradient differed from the typical value. The total ozone was equal to  $X\sim 300$  DU at  $H=0\text{km}$ ,  $X\sim 240$  DU at  $H>3$  km  
 651 and  $X\sim 250$  DU at  $H\sim 1-2$  km.

652 Fig.8. Total UV amplification as a function of the altitude for different types of BAUVR in a variety of atmospheric  
 653 conditions with  $S=0$  (a) and  $S=0.9$  (b). The model parameters at  $H=0$  km:  $X=250-350$  DU,  $AOD_{340}=0.2-0.4$ . The  
 654 Alpine type of AOD altitude dependence according to the Eq. (15) was taken into account. Solar elevation  $h=50^\circ$ .

655 Fig.9. The UV amplification due to molecular  $A_M(Q_{ery})$ ,  $A_M(Q_{vitD})$ , ozone  $A_X(Q_{vitD})$ ,  $A_X(Q_{ery})$ , aerosol  $A_{AOD,fl(H)}$ ,  
 656  $A_{AOD,f2(H)}$  for the Alpine  $f1(H)$  and Asian  $f2(H)$  types of altitude dependences, and surface albedo  $A_S(Q_{ery})$ ,  $A_S(Q_{vitD})$   
 657 changes with the altitude (a) and their total altitude effect on  $A_{UV}$  for different types of BAUVR (b). At  $H=0$  km:  
 658  $AOD_{340}=0.8$ ,  $X=250$  DU. The surface albedo has an abrupt change at 2 km from  $S=0$  to  $S=0.95$ . Solar elevation -  
 659  $h=50^\circ$ .

660 **LIST OF THE TABLES:**

661

662 Table 1. Relative molecular gradients  $G_{bio\_M(A=0)}$  (%/km) at different solar elevations and ozone content for different  
 663 types of BAUVR. Accurate model simulations. Zero surface albedo conditions. Determination coefficient  $R^2$  is  
 664 higher than 0.997 in all cases. The standard error of  $G_{bio\_M(A=0)}$  is given in the brackets at P=95% .

665

h, solar elevation, degrees	erythemally-weighted irradiance	cataract-weighted irradiance	vitamin D-weighted irradiance	erythemally-weighted irradiance	cataract-weighted irradiance	vitamin D-weighted irradiance
	X=300 DU			X=500 DU		
10	4.5 (0.04)	3.8 (0.04)	1.8 (0.01)	4.8 (0.05)	3.9 (0.04)	0.8 (0.03)
20	6.4 (0.04)	6.9 (0.05)	7.1 (0.06)	6.0 (0.03)	6.6 (0.04)	6.8 (0.05)
30	6.7 (0.01)	7.2 (0.02)	7.8 (0.02)	6.1 (0.01)	7.0 (0.01)	7.8 (0.02)
40	6.4 (0.02)	6.8 (0.01)	7.3 (0.01)	5.8 (0.02)	6.6 (0.02)	7.4 (0.01)
50	6.0 (0.03)	6.2 (0.03)	6.7 (0.03)	5.5 (0.03)	6.1 (0.03)	6.8 (0.03)
60	5.7 (0.04)	5.8 (0.04)	6.2 (0.04)	5.3 (0.04)	5.7 (0.04)	6.4 (0.04)

666

667

668 Table 2. The coefficients for calculating the  $r_{bio}$  values (Eq. 21) for different types of BAUVR. Model estimations.

669 The standard error of the coefficients is given in the brackets at P=95%.

	erythemally-weighted irradiance	cataract-weighted irradiance	vitamin D-weighted irradiance
$b$	-0.025(0.0002)	-0.025(0.0002)	-0.025(0.0002)
$c$	0.394(0.0009)	0.394(0.0009)	0.405(0.0008)
$R^2$	>0.99	>0.99	>0.99

670 Note: the simulations were fulfilled for different combinations of input parameters at  $H=0$ :

671  $X=250-350$  DU,  $AOD_{340}=0.2-0.4$ ,  $S=0-0.9$ ,  $h=20-50^\circ$ .

672

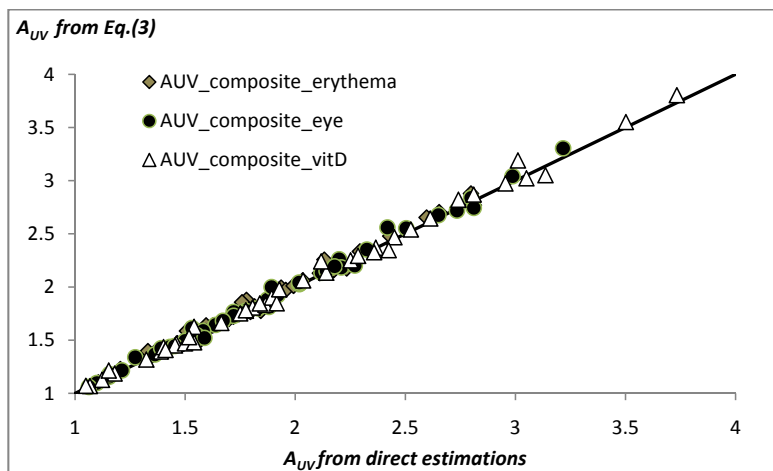
673

674



675 FIGURES

676



677

678

679

680 **Figure 1.** The comparison of  $A_{UV}$  amplification factor calculated from Eq.(4) as multiplication of  $A_M A_X A_{AOD} A_S$  with the  
681 direct model simulation of UV amplification. All the parameters ( $A_{UV}, A_M A_X A_{AOD} A_S$ ) were obtained from accurate model  
682 simulations.

683 *Comment.* The simulations were performed for different altitudes ( $H=0$  and  $H=5\text{km}$ ), aerosol optical depth ( $AOD_{340}=0, 0.2,$   
684  $0.4$ ), total ozone ( $X=250,300,350$  DU), surface albedo ( $S=0, S=0.9$ ) and solar elevations ( $h=20^\circ$  and  $50^\circ$ ). For estimating the  
685 UV amplification we assume at  $H=0$  km the conditions with  $350\text{DU}, AOD_{340}=0.4, S=0\%$  and normalized the BAUVR at the  
686 altitude  $H=5\text{km}$  to the value calculated with these parameters.

687

688

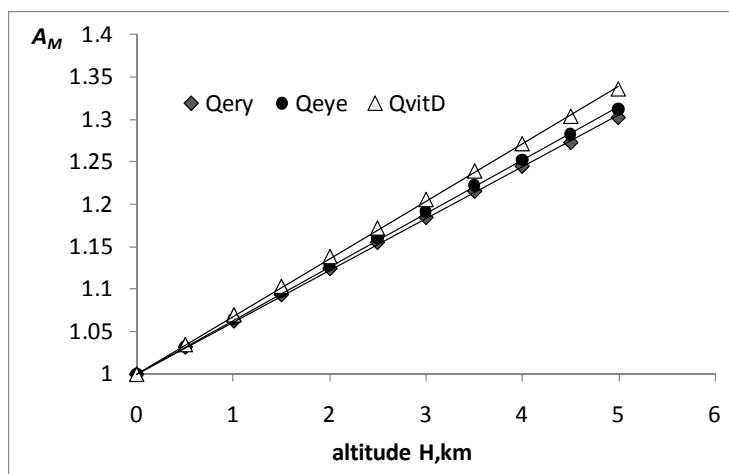
689

690

691



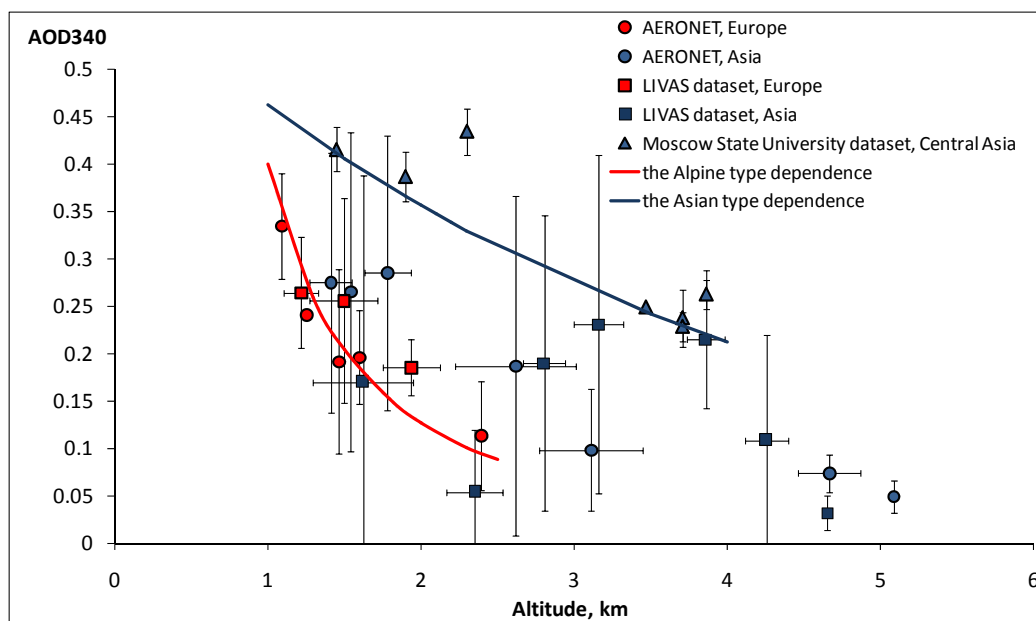
692  
693  
694  
695  
696  
697  
698  
699  
700  
701  
702  
703  
704  
705  
706  
707  
708  
709  
710



711 **Figure 2. UV amplification due to decrease in molecular number density with the altitude  $H$  according to accurate**  
712 **model simulations: 8- stream DISORT TUV model.  $h=50^\circ$ .  $X=300$  DU.  $R^2>0.997$  – for all regression lines.**  
713  
714  
715



716



717

718

719

720

721

722

723

724

725

726

727

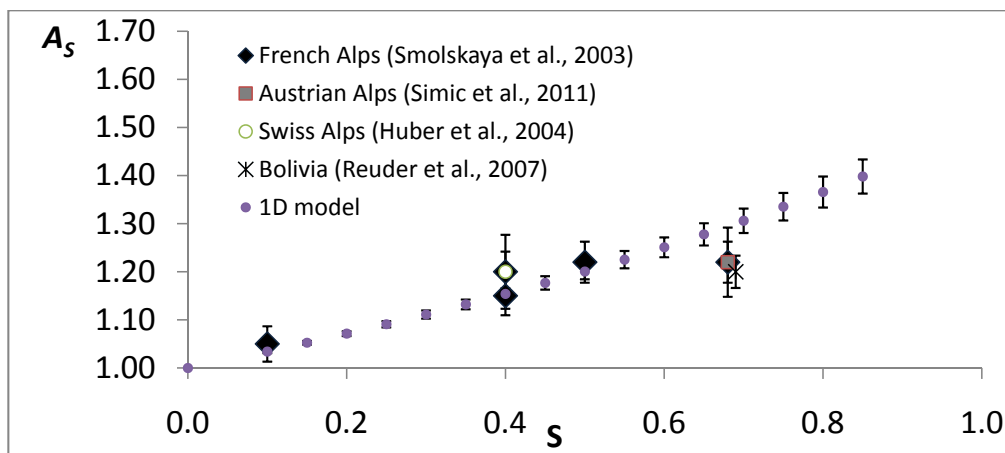
728

729

Figure 3. The altitude dependence of aerosol optical depth at 340nm with 1 sigma error bar according to the AERONET, LIVAS and the Moscow State University datasets over European and Asian regions. May-September period. The AOD at 330 nm the Moscow State University dataset and the AOD at 355nm from the LIVAS datasets were recalculated to AOD at  $\lambda=340$  nm using the Angstrom parameter  $\alpha=1.3$ . See further details in the text.



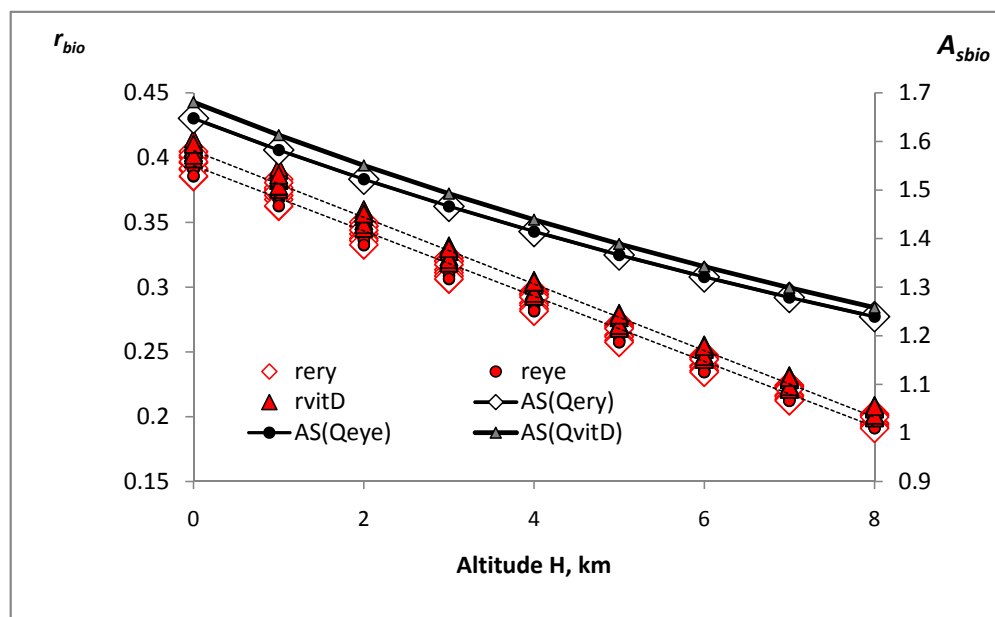
730  
731



732

733 **Figure 4. UV amplification due to the surface albedo increase in mountainous areas according to different**  
734 **experimental data and model simulations. The error bars of model simulation relates to the different input**  
735 **parameters – altitude of 2 and 3 km, solar elevation of 10, 30 and 50°, total ozone X=350DU, AOD<sub>340</sub>=0.17 at**  
736 **P=95%.**

737  
738  
739  
740  
741  
742  
743



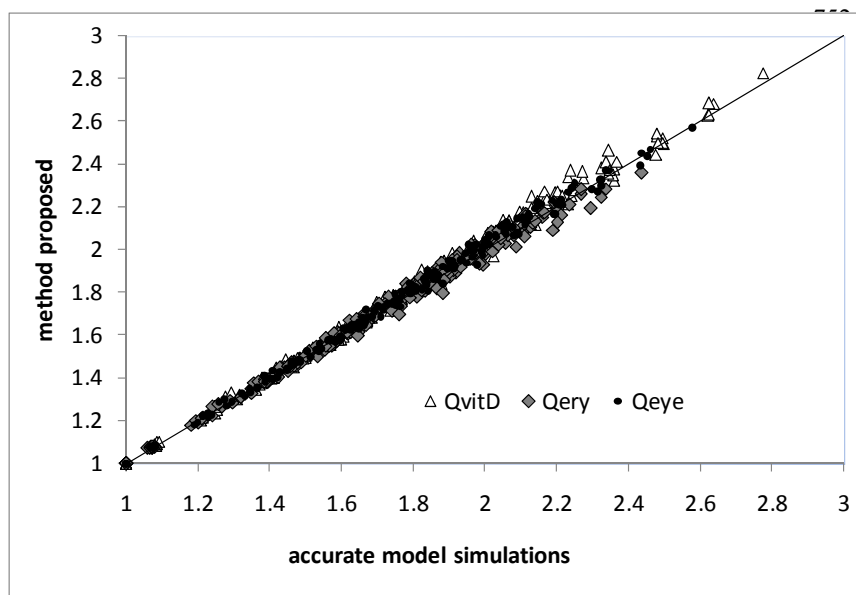
744

745 Figure 5. The dependence of  $r_{bio}$  with the altitude for different BAUVR from accurate model simulations for a  
 746 variety of geophysical parameters (left axis) and maximum  $A_s$  effects due to changes in surface albedo from  $S=0$  at  
 747  $H=0$  km to  $S=1$  at level  $H$  (right axis). The  $r_{bio}$  regressions are shown in dashed line. Note, that the regression line for  
 748  $r_{O_{eye}}(H)$  is the same as for  $r_{O_{ery}}(H)$ . The coefficients of the regression equations and the ranges of the input  
 749 parameters at  $H=0$  are given in Table 2.

750



751



768

769

770

771 **Figure 6. The comparison between the total altitude UV amplification ( $A_{UV}$ ) according to the proposed method and**  
772 **the  $A_{UV}$  values evaluated using the accurate RT model (TUV, 8-stream DISORT method).**

773

774

775

776

777

778

779

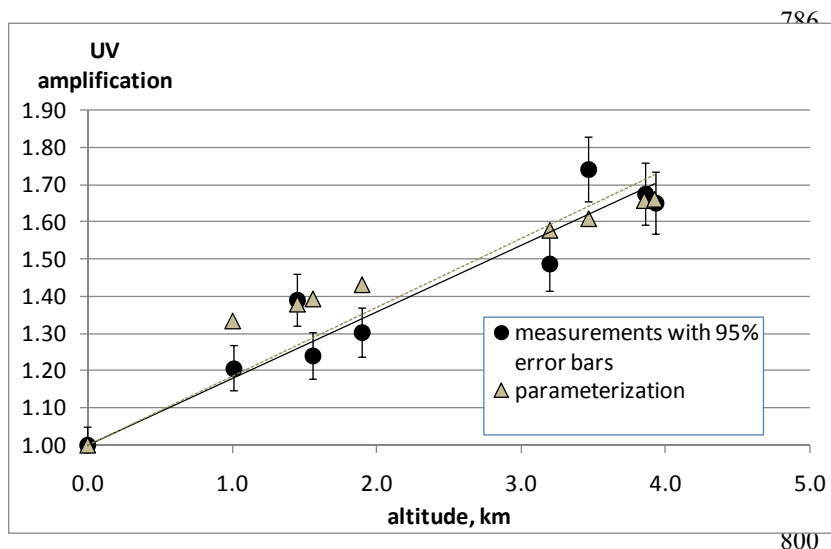
780

781

782



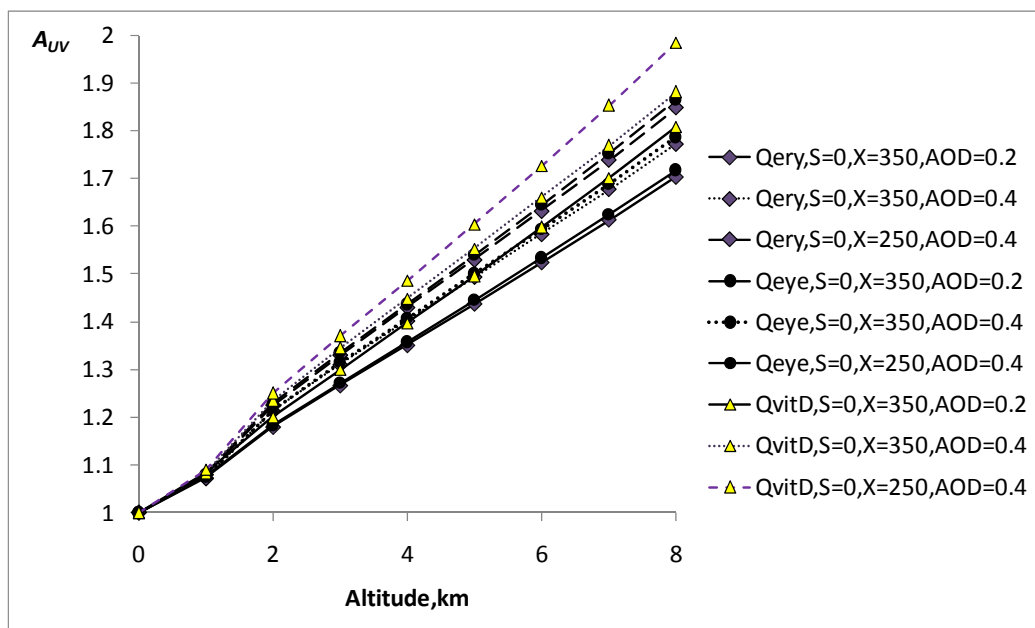
783  
784  
785



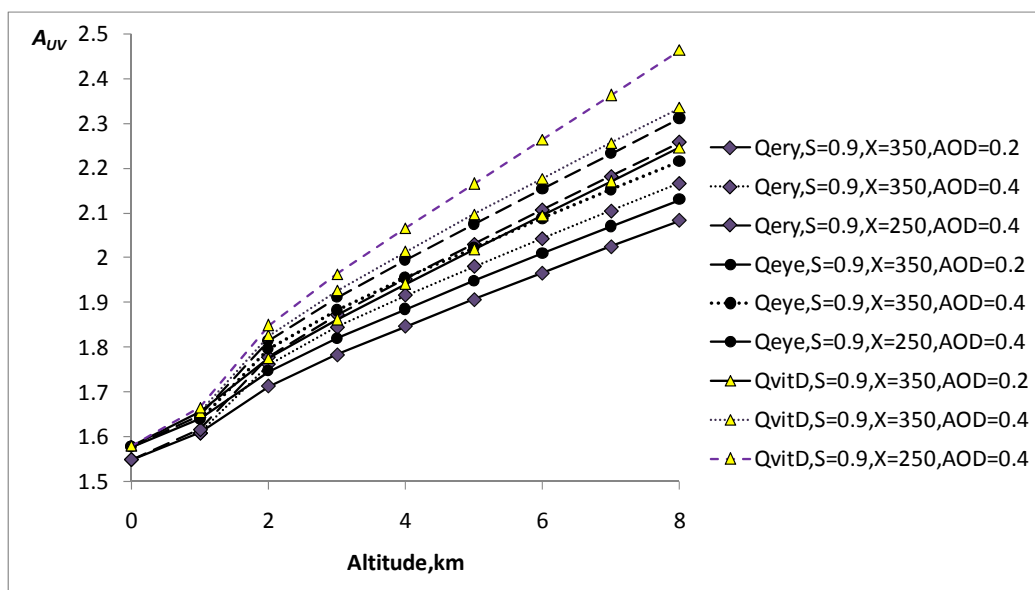
801  
802  
803

804 **Figure 7.** The comparison between the simulated UV amplification according to the proposed parameterization and  
805 the UV amplification from the experimental data as a function of altitude. Moscow State University dataset. Solar  
806 elevation  $h=50^\circ$ . Clear sky conditions. Note: since we used the data of different field campaigns the ozone altitude  
807 gradient differed from the typical value. The total ozone was equal to  $X\sim 300$  DU at  $H=0$  km,  $X\sim 240$  DU at  $H>3$  km  
808 and  $X\sim 250$  DU at  $H\sim 1-2$  km.

809  
810  
811  
812  
813  
814  
815



816 a/  
 817



818 b/

819 **Figure 8.** Total UV amplification as a function of the altitude for different types of BAUVR in a variety of  
 820 atmospheric conditions with  $S=0$  (a) and  $S=0.9$  (b). The model parameters at  $H=0$  km:  $X=250-350$  DU,  $AOD_{340}=0.2-$   
 821  $0.4$ . The Alpine type of AOD altitude dependence according to the Eq. (15) was taken into account. Solar elevation-  
 822  $h=50^\circ$ .

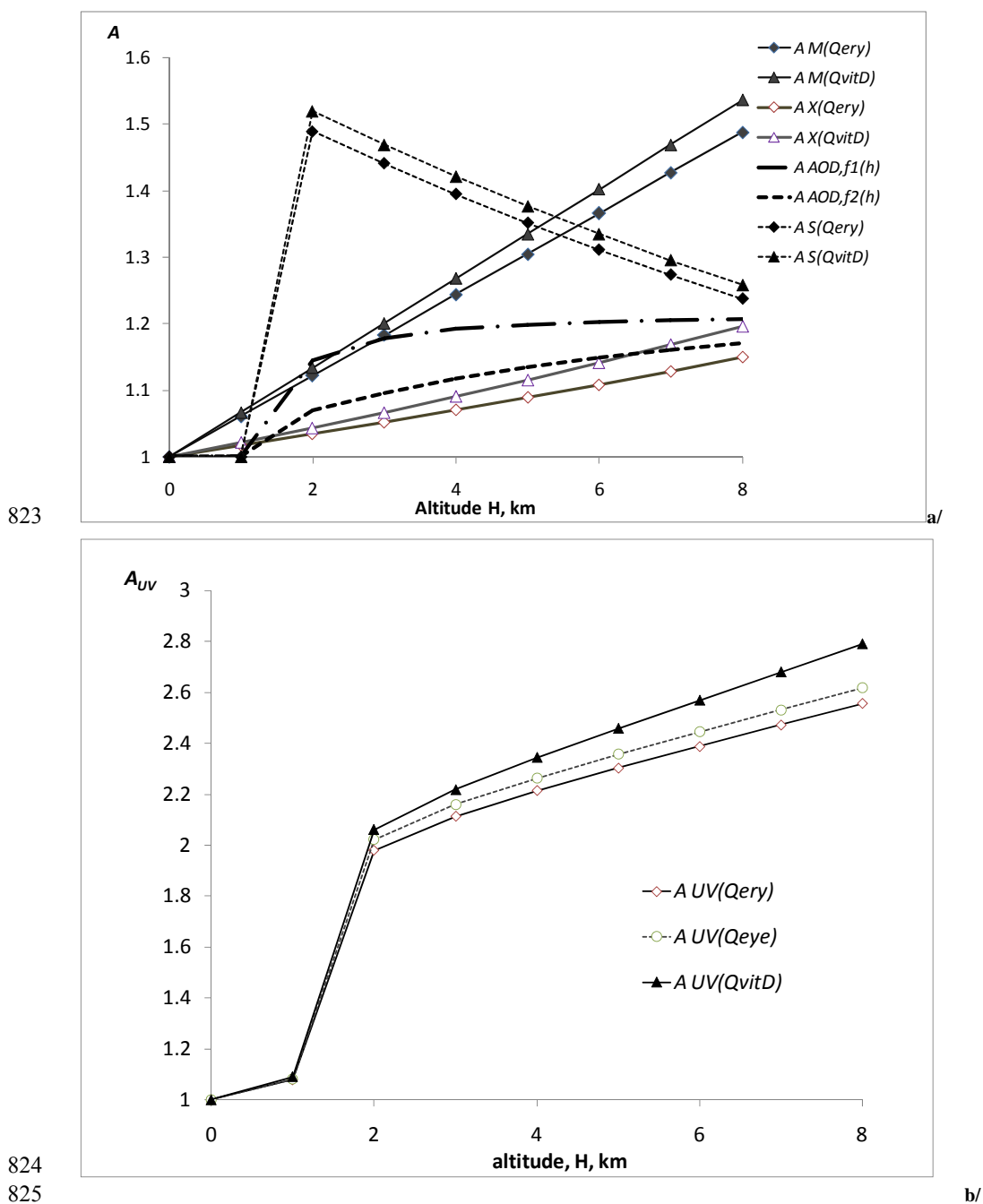


Figure 9. The UV amplification due to molecular  $A_M(Qery)$ ,  $A_M(QvitD)$ , ozone  $A_X(QvitD)$ ,  $A_X(Qery)$ , aerosol  $A_{AOD, f1(H)}$ ,  $A_{AOD, f2(H)}$  for the Alpine  $f1(H)$  and Asian  $f2(H)$  types of altitude dependences, and surface albedo  $A_S(Qery)$ ,  $A_S(QvitD)$  changes with the altitude (a) and their total altitude effect on  $A_{UV}$  for different types of BAUVR (b). At  $H=0$  km:  $A_{OD_{340}}=0.8$ ,  $X=250$  DU. The surface albedo has an abrupt change at 2 km from  $S=0$  to  $S=0.95$ . Solar elevation -  $h=50^\circ$ .